



OPEN

Biodegradable porous micro/nanoparticles with thermoresponsive gatekeepers for effective loading and precise delivery of active compounds at the body temperature

Kamonchanok Thananukul^{1,2}, Chariya Kaewsaneha¹, Pakorn Opaprakasit¹✉, Nadia Zine² & Abdelhamid Elaissari²✉

Stimuli-responsive controlled delivery systems are of interest for preventing premature leakages and ensuring precise releases of active compounds at target sites. In this study, porous biodegradable micro/nanoparticles embedded with thermoresponsive gatekeepers are designed and developed based on Eudragit RS100 (PNIPAM@RS100) and poly(N-isopropylacrylamide) *via* a double emulsion solvent evaporation technique. The effect of initiator types on the polymerization of NIPAM monomer/methylene-bis-acrylamide (MBA) crosslinker was investigated at 60 °C for thermal initiators and ambient temperature for redox initiators. The crosslinked PNIPAM plays a key role as thermal-triggered gatekeepers with high loading efficiency and precise release of a model active compound, Nile Blue A (NB). Below the volume phase transition temperature (T_{VPT}), the gatekeepers possess a swollen conformation to block the pores and store NB within the cavities. Above its T_{VPT} , the chains rearrange, allowing gate opening and a rapid and constant release rate of the compound until completion. A precise “on–off” switchable release efficiency of PNIPAM@RS100 was demonstrated by changing the temperatures to 4 and 40 °C. The materials are a promising candidate for controlled drug delivery systems with a precise and easy triggering mechanism at the body temperature for effective treatments.

Smart delivery systems have attracted growing attention for selective delivery of active compounds, especially therapeutic agents, to targeted disease tissues. Smart drug delivery carriers are designed to deliver drugs without premature leakage and rapidly release loaded drugs after being uptaken by internal and external stimuli¹. Stimuli-responsive drug delivery systems have crucial functions in responding to biological environment stimuli, such as pH², temperature³, electric or magnetic field⁴, light⁵, enzyme⁶, and biological stimuli⁷. These systems can be applied externally and remotely to achieve controlled release from the drug carriers.

Various micro- and nano-particles have been employed in biomedical/pharmaceutical fields for effective treatments by improving the bioavailability and longevity of specific therapeutic in the blood system and increasing its accumulation at the biological target (thus reducing side effects)⁸. Microparticles are typically useful as reservoir systems for the controlled release of drugs, including polypeptide/protein drugs. At the same time, nanoparticles are suitable for intravenous injection administration, aiming at a cellular/subcellular target^{9,10}. Chen et al. reported that large-sized microparticles of gefitinib-loaded poly(lactic-*co*-glycolic acid) (PLGA) showed a prolonged release mechanism¹¹. Kim et al. fabricated highly porous PLGA particles ($11.5 \pm 0.4 \mu\text{m}$) loaded

¹School of Bio-Chemical Engineering and Technology, Sirindhorn International Institute of Technology (SIIT), Thammasat University, Pathum Thani 12121, Thailand. ²Univ Lyon, University Claude Bernard Lyon-1, CNRS, ISA-UMR 5280, 69622 Villeurbanne, France. ✉email: pakorn@siit.tu.ac.th; abdelhamid.elaissari@univ-lyon1.fr

with tumor-drug for lung cancer treatment *via* an inhalation route¹². The PLGA-based microparticles gradually released the drugs over 7 days. Pulmonary administration of the microparticles resulted in their deposition in mouse lungs and remained for up to a week. Reczyńska et al. reported that microparticles with diameters between 2 and 3.5 μm with a narrow size distribution could increase the effectiveness of their deposition in deeper parts of the respiratory tract¹³. Nanoparticles provide additional advantages in precisely delivering active compounds to a specific target. This is particularly of interest as chemotherapy drug carriers. Tian et al. developed high potential chemo- and magnetic hyperthermia therapeutic platforms based on thermoresponsive copolymers coated magnetic mesoporous silica nanoparticles (MSN)¹⁴. The nanoparticles showed low cytotoxicity and could be internalized by HeLa cells. The nanoparticles loading with doxorubicin (Dox) exhibited a synergistic effect of chemo- and magnetic hyperthermia therapy, resulting in higher efficacy in killing cancer cells. Similarly, Dox-loaded mesoporous silica nanoparticles functionalized with poly(ethylene glycol)/poly(ϵ -caprolactone) (PEG/PCL) multiblock copolymer were prepared and used for heat-shock drug delivery system. In response to heat shock stimuli (45 °C), Dox was released from the functionalized MSN particles due to the loosening of the structure of the gatekeeper, PEG/PCL, leading to effective killing of tumor cells¹⁵.

The development of an efficient encapsulation process, especially for drug carriers, aims to protect the entrapped active agents against light, oxidation, and enzyme degradations¹⁶. Among drug carriers explored, porous particles have remarkable properties, such as large surface area, high porosity, high uniformity, tunable pore structures, and surface modifiability¹⁷. Porous cavities can efficiently encapsulate various active compounds with high loading capacity. The particles can be fabricated by both inorganic (mesoporous silica particles)¹⁸ and organic materials, e.g., poly(lactic acid-co-glycolic acid), poly(methyl methacrylate), polylactic acid, and ammonio methacrylate copolymer (Eudragit RS100)^{19–21}. Biodegradable Eudragit RS100 was fabricated as porous particles by a double emulsion (W/O/W) solvent evaporation method. A two-step emulsification process was employed for porous particle formation. The water-in-oil (W_1/O) emulsion was formed by dispersing the inner aqueous phase (W_1) in organic solvent (O), and emulsifying the primary emulsion in the continuous aqueous phase (W_2). Zafar et al. reported the fabrication of sponge-like Eudragit RS100 particles *via* a double emulsion solvent evaporation process. The obtained particles possessed porous structures because of the interaction between positively-charged ammonium groups of the polymer and the water molecules. This led to the formation of hydrophilic cavities after solvent evaporation²¹.

Incorporating stimuli-responsive polymers onto porous carriers has been designed to accomplish controlled release formulations by employing the porous particles as hosts and stimuli-responsive polymers as gatekeepers. A gatekeeper can provide the pores' close/open switchable function when triggered. Various temperature-sensitive gatekeepers have been vastly investigated due to their specific sol-gel phase transition temperatures. Among these, poly(*N*-isopropylacrylamide) (PNIPAM) possesses a lower critical solution temperature (LCST) at around 32 °C in an aqueous solution. Below the LCST, PNIPAM is swollen due to hydrogen bond formation between its amide groups and water molecules. Above LCST, however, the polymer segments become hydrophobic and shrunk^{22,23}. When PNIPAM is crosslinked in the form of hydrogels, the critical temperature is called volume phase transition temperature (T_{VPT})²². Su et al. prepared thermo-responsive composites of hollow silica particles with ordered mesoporous shell coated with PNIPAM layer as a thermo-responsive gate. PNIPAM corona was formed surrounding the hollow silica particles *via* an *in situ* polymerization. The uptake and release of rhodamine B (a model compound) were examined to assess the stimuli-responsiveness of the composite particles. The uptake and release behaviors were observed at 25 °C (<LCST), while the dehydrated hydrophobic polymer layer collapsed over the particle surface at 50 °C (>LCST), leading to a shutoff of the uptake and release²⁴. Although the silica-PNIPAM composite particles showed advantages from the hollow mesoporous silica structure and the thermo-responsive polymer gating, a multi-step preparation process is required.

Biodegradation and biocompatibility are essential for materials to use in drug delivery systems. Although PNIPAM has low biodegradability, its application as a structural modifier or co-polymerization with other biodegradable polymers increases their degradation rate²⁵. In addition, PNIPAM has been proven a biocompatible polymer. Capella et al. synthesized PNIPAM hydrogels *via* free radical polymerization, whose biocompatibility was assessed on mouse preadipocytes cells, human embryonic kidney cells 293, and human lung carcinoma epithelial cells²⁶. The cell viability results reflected non-cytotoxicity after 96 h. In a separate study, the biocompatibility of PNIPAM nanoparticles at a high concentration (1000 mg/mL) was examined on two mammalian cell lines, i.e., human keratinocyte (HaCaT) and colon cells (SW480)²⁷. The nanoparticles didn't elicit cytotoxic responses in either HaCaT or SW480 cells, indicating their high biocompatibility. Upon internalization, the particles were engulfed in lysosomes, rendering them effectively harmless. In addition, Eudragit RS100 nanoparticles have been shown to elicit no cytotoxicological responses in SW480 cells, although internalized, suggesting their potential as nanocarriers to the drug delivery system.

In the present work, thermally-sensitive micro- and nanoparticles derived from Eudragit RS100 and PNIPAM (PNIPAM@RS100) are designed to achieve a smart delivery system. PNIPAM is selected as a gatekeeper owing to its extensive biocompatibility and cellular interaction to cover the pores of Eudragit RS100 to block the diffusion of active molecules, especially drugs, with a thermal responsive triggering mechanism. The crosslinked PNIPAM nanogels are polymerized during the formation of Eudragit RS100 porous particles by double emulsion solvent evaporation. The PNIPAM nanogels are then decorated in the cavities of the porous particles to act as gatekeepers. The formation mechanism of the thermoresponsive gates is examined. The effect of chemical initiators on the degree of polymerization of NIPAM in the presence of methylene bis-acrylamide (MBA) crosslinker is investigated at 60 °C for ammonium persulfate (APS) and room temperature for redox initiators (APS/TEMED). The hydrodynamic particle size and electrophoretic mobility were measured to determine the volume phase transition temperature of the crosslinked PNIPAM nanogels. Nile Blue A (NB) is then employed as a model compound. The loading efficiency and releasing behavior of NB-loaded PNIPAM@RS100 are examined to assess their performance in smart, responsive, controlled release applications.

Experimental

Materials. Ammonio methacrylate copolymer type BNF (Eudragit RS100), a molecular weight of 32,000 g/mol, was purchased from Evonik, Germany. *N*-isopropylacrylamide (NIPAM) (99% pure) and ammonium persulfate (APS) were purchased from Acros Organics and Bio-Rad, respectively. Dichloromethane (DCM), *N,N,N',N'*-tetramethylethylenediamine (TEMED, ≥ 99%), *N,N'*-methylenebisacrylamide (MBA, 99%), and Nile Blue A (NB) were purchased from Sigma-Aldrich. Deionized water was used throughout this work. Chemical structures of the main components of thermoresponsive gating particles are shown in Supplemental Fig. S1.

Preparation of thermoresponsive gating particles (PNIPAM@RS100). Thermoresponsive gating micro-/nanoparticles (PNIPAM@RS100) were obtained *via* the double emulsion solvent evaporation method. The thermoresponsive components of NIPAM (0.2 g, MBA (0.02 g), APS (0.01 g), and TEMED (10 μL) were dissolved in 2 mL of an internal aqueous phase (W_1). Eudragit RS100 (1 g) was dissolved in 5 mL dichloromethane organic solvent (O). The aqueous phase was emulsified in the organic phase using an ultrasonicator (Optic ivymen system CY-500) at an amplitude 70% for 2 min. The primary emulsion (W_1/O) was transferred to 50 mL of an external aqueous phase (W_2) and homogenized using either Ultra-Turrax (IKA-Werke T25 basic) at 13,500 rpm or ultrasound at amplitude 70% for 10 min. The obtained double emulsion ($W_1/O/W_2$) was evaporated by a rotary evaporator (Nahita model 9300), as shown in Supplemental Fig. S2. PNIPAM@RS100 was purified through centrifugation (Fisherbrand, GT2R Centrifuge) at 5000 rpm for 10 min and washed with DI water to remove residue water-soluble PNIPAM.

The effect of initiator systems on the PNIPAM gatekeeper formation was examined. The redox initiating system involving APS as an initiator and TEMED as a catalyst was employed, as the polymerization of NIPAM can be initiated at room temperature *via* a double emulsion technique. This was compared with APS thermal initiator, which decomposes and generates free radicals at 60 °C for 6 h.

Characterizations. The particle size and zeta potential of the prepared PNIPAM@RS100 were determined by a microelectrophoresis apparatus (Zetasizer; Malvern, Nano ZS). The samples were diluted and dispersed in 1 mM NaCl before measurements. The particle size and zeta potential of each sample as a function of temperature were measured at a temperature range of 25–55 °C. Each measurement was performed in triplicate. The particle morphology was examined using a transmission electron microscope (TEM; JEOL, JEM-2100 Plus), operated at an accelerating voltage of 200 kV, and a scanning electron microscope (SEM; JEOL, JSM7800F), acquired after gold sputtering at an acceleration voltage of 10 kV. The chemical structures and functional groups of the prepared particles were analyzed by Fourier transform infrared (FTIR) spectrometer in an attenuated total reflection mode (ATR-FTIR; Nicolet iS50, Thermo Scientific).

The volume phase transition temperature of PNIPAM nanogels. PNIPAM nanogels were synthesized by free-radical polymerization in a surfactant-free process to determine the volume phase transition temperature (T_{VPT}). In the reaction flask, 0.2 g of NIPAM monomer and 0.02 g of MBA crosslinking agent were dissolved in 20 mL distilled water by stirring with a magnetic bar for 30 min. The temperature was then raised to 70 °C. Subsequently, 10 mg APS was added to the solution to initiate the reaction. The polymerization was carried out at 70 °C for 4 h. The solution became turbid after mixing. The unreacted monomers were separated using a centrifuge filter (0.1 μm pore size). T_{VPT} was investigated by measuring the hydrodynamic particle size as a function of temperature from 25 to 55 °C, after being diluted in 1 mM NaCl medium. The electrophoretic mobility (μ) of the particles was measured as a function of temperature using a Zetasizer. The swelling ratio of the nanogels is defined as the volume of swollen PNIPAM nanogels (equilibrium swelling at 25 °C) divided by that of the collapsed state (at 55 °C) according to the following equation²⁸.

$$\text{Swelling ratio} = \left(\frac{D_s}{D_c} \right)^3 \times 100 \quad (1)$$

where D_s and D_c are average hydrodynamic diameters of nanogels in the swollen and collapsed states, respectively.

Embedding of PNIPAM gatekeepers into porous particles. The content of the PNIPAM gatekeepers in the porous particles was determined by calculating the percentage of NIPAM conversion. The unreacted NIPAM monomer in the emulsion was collected by centrifugation. The supernatant was dried, whose chemical structures were examined by FTIR spectroscopy. The results confirm that the compounds suspended in the supernatant are NIPAM monomer residues, as shown in Supplemental Fig. S3. Finally, the mass of the polymerized PNIPAM, and % conversion were evaluated by using Eqs. (2) and (3), respectively

$$M_i = M_{wps} + M_p \quad (2)$$

$$\% \text{Conversion} = \frac{M_p}{M_i} \times 100 \quad (3)$$

where M_i is the mass of the initial monomer, M_{wps} is the mass of dried unreacted monomer in the supernatant, and M_p is the mass of polymerized PNIPAM.

Encapsulation efficiency and loading capacity. NB is employed as a model compound in the encapsulation process. NB (1 mg/mL) was added to the primary aqueous solution (W_1), before PNIPAM@RS100 for-

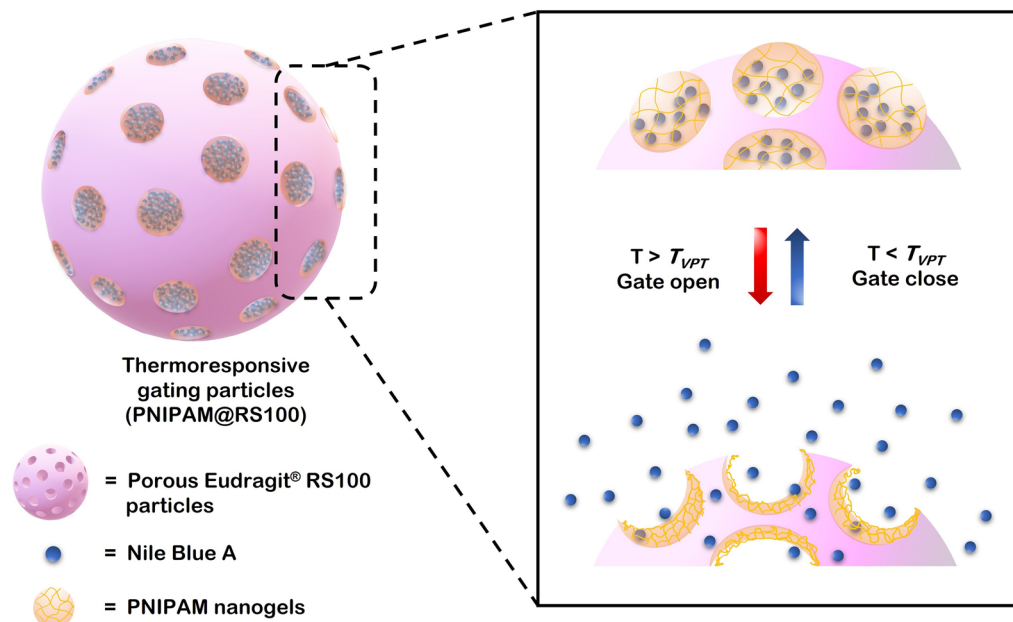


Figure 1. Design of thermoresponsive gating particles and the controlled release mechanism of thermally sensitive PNIPAM gatekeepers.

mation. The encapsulated particles were centrifuged to separate the particles and the supernatant. The collected supernatant was analyzed using a UV-Vis spectrophotometer (UV-1800, Shimadzu) at 635 nm. All samples were measured in triplicate. The encapsulation efficiency (%EE) and loading capacity (%LC) were calculated using Eqs. (4) and (5), respectively.

$$\%EE = \frac{\text{Initial amount of NB} - \text{Amount of NB in supernatant}}{\text{Initial amount of NB}} \times 100 \quad (4)$$

$$\%LC = \frac{\text{Initial amount of NB} - \text{Amount of NB in supernatant}}{\text{Weight of nanoparticles}} \times 100 \quad (5)$$

Controlled release mechanism. In the study of NB release behavior, 0.2 mg of NB-loaded PNIPAM@RS100 was suspended in distilled water. A drop (5 μ L) of 0.1 M hydrochloric acid (HCl) was added into the releasing medium to aid the observation of NB color. The real-time NB release was monitored continuously using a UV-Vis spectrophotometer (UV-1800, Shimadzu) at 635 nm for 5 h, at 25.0 ± 0.5 and 37.0 ± 0.5 $^{\circ}$ C. Finally, the cumulative release was determined from a standard calibration curve (Supplemental Fig. S4).

The switchable close/open gating properties of the materials were evaluated by incubating at 4 and 40 $^{\circ}$ C. The crosslinked PNIPAM gatekeepers were turned off at a low temperature (4 $^{\circ}$ C) for 5 min and turned on for 5 min allowing NB to release above the T_{VPT} (40 $^{\circ}$ C). This process was repeated for four cycles. The released NB content was calculated.

Results and discussion

Design and formation of thermoresponsive gating particles (PNIPAM@RS100). A schematic representation of the thermoresponsive PNIPAM gating system for controlled delivery is shown in Fig. 1. The porous domain structure of Eudragit RS100 was successfully prepared without any stabilizer, as reported in the literature²¹. The PNIPAM gates were produced during the PNIPAM@RS100 formation *via* a double emulsion solvent evaporation. In the first step, water-soluble compounds of thermoresponsive gates and NB were dissolved in the aqueous inner W_1 phase, then dispersed into the organic phase. The W_1/O nanodroplets were converted into PNIPAM nanogels after polymerization, and NB was encapsulated inside the nanogels. A double emulsion ($W/O/W$) was formed by dispersing the primary emulsion in a secondary water phase (W_2). Finally, the organic solvent was evaporated, resulting in the formation of PNIPAM@RS100.

The NB model compound was encapsulated within the PNIPAM nanogels in the porous Eudragit RS100 particles. Upon increasing the temperature above T_{VPT} , a collapse in the PNIPAM network structure leads to an opening of the pores and a release of the model compound.

Structure and properties of PNIPAM gatekeepers. PNIPAM nanogels were fabricated by radical polymerization to determine T_{VPT} of the thermally-sensitive gatekeepers. The results on average particle sizes

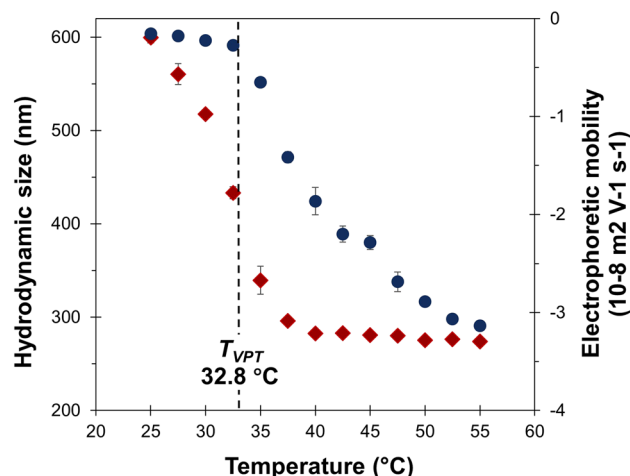


Figure 2. The effect of temperature on hydrodynamic particle size (red rhombus) and electrophoretic mobility (dark blue circle) of the crosslinked thermally-sensitive nanogels.

of the PNIPAM nanogels as a function of temperature from 25 to 55 °C are summarized in Fig. 2. All samples showed monodisperse size distribution with a polydispersity index (PDI) < 0.1. This indicates that the hydrodynamic diameter tends to decrease with increasing temperature. T_{VPT} was calculated from the first derivative of the first transition step (start to collapse, around 27 °C), and the second transition at around 40 °C, using a polynomial fitting^{29,30}. Therefore, the observed T_{VPT} is at 32.8 °C. The variation in the temperature plays a key role in the hydrodynamic size of the crosslinked nanogels. The swelling and shrinking behaviors are due to the breaking of hydrogen bonds between PNIPAM networks and water molecules during the temperature escalation, resulting in a decrease in the particle's hydrodynamic size³¹.

The swelling ratio is defined as a ratio between the volumes of the nanogels in the swollen and the collapse states. At 1% of MBA crosslinker content, the swelling ratio of the prepared nanogels was 10.5. The swelling ratio is related to the crosslink density of the hydrogels. The increase in the crosslinker concentration leads to higher crosslink density. However, the water absorption capacity is reduced^{28,32}. In addition, T_{VPT} of the thermally-sensitive particles is dependent on the monomer types and the monomer/crosslinker ratio. Varga et al.³³ reported that an increase in the crosslink density reduced the swelling behavior of PNIPAM microgel particles and shifted their T_{VPT} value, as a result of crosslinker content differences. The sol–gel transition was observed upon temperature changes. The nanogels form a sol phase at room temperature or below T_{VPT} while at temperatures higher than T_{VPT} , these become hydrophobic or a gel phase due to hydrogen bonding disruption, leading to a turbid solution^{29,34}.

The electrophoretic behavior reflects the motion of thermosensitive particles under external electric and friction forces due to their charge density³⁵. Figure 2 also demonstrates the electrophoretic mobility of PNIPAM particles as a function of temperature. The negative electrophoretic mobility values indicated that these nanogels were negatively charged inherited from sulfate groups of the APS anionic initiator. The results on the effect of cationic and anionic initiators on the surface charge density and electrophoretic mobility of the particles agree with those previously reported³⁰. Below T_{VPT} (at 32.8 °C), the electrophoretic mobility of nanogels was near zero with negatively charged, because of the low surface charge density of the swollen particles. The change in electrophoretic mobility was observed when the temperature was increased above T_{VPT} . The value also increased with the decrease of particle diameter, as the charges located on the hydrodynamic surface were closer to each other, leading to an increase in the surface charge density. This phenomenon is likely because the shrinkage of particles induces the reorganization of the charged groups, and enhances the surface charge density^{30,36}. The relationship between temperature and electrophoretic mobility can be explained by the Helmholtz–Smoluchowski's equation^{37,38}, in which the electrophoretic mobility (μ_e) is correlated with the surface charge density (σ) and hydrodynamic particle size ($2r_h$), as follows:

$$\mu_e \approx \frac{Ne}{4\pi\eta\kappa r_h^2} \quad (6)$$

where N is the number of charge groups, e is the electronic charge, η is the viscosity of the medium, and κ is the reciprocal Debye length.

Structure and properties of thermoresponsive gating particles (PNIPAM@RS100). The formation of thermoresponsive gating porous particles (PNIPAM@RS100) was obtained by the double emulsion (W/O/W) solvent evaporation technique. The double emulsion was prepared *via* a two-step emulsification process, in which a primary (W_1/O) emulsion was employed to form PNIPAM gatekeeper nanogels. These were then dispersed in Eudragit RS100 solution to formulate a double emulsion ($W_1/O/W_2$). The primary emulsion as the oil phase was transferred to another aqueous phase under a high-speed homogenizer ultra turrax (UT) or

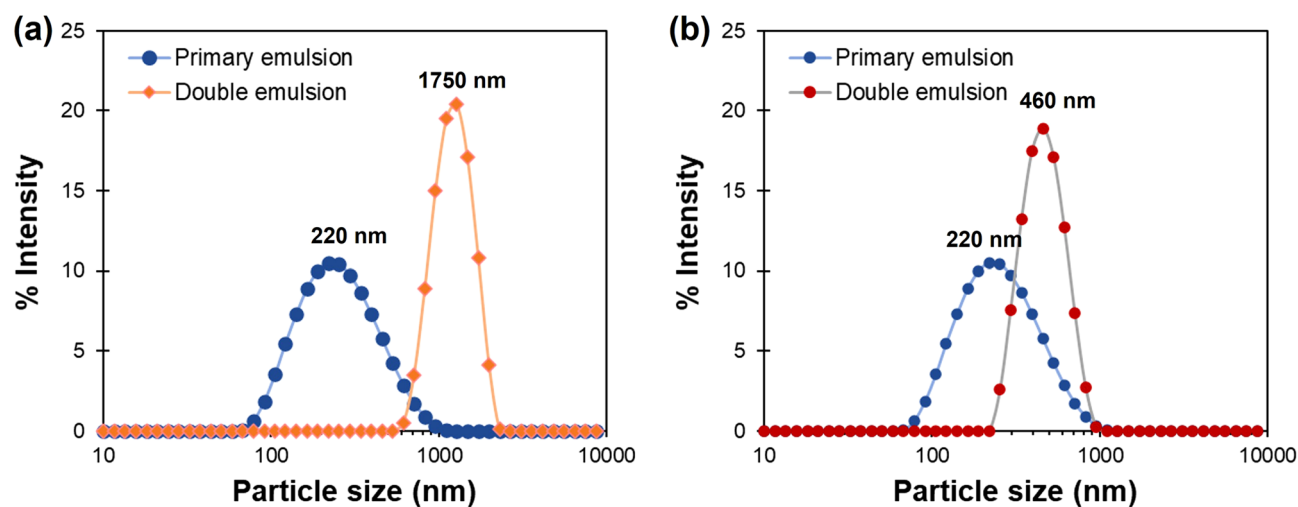


Figure 3. Particle size distribution of a primary W_1/O emulsion and a double $W_1/O/W_2$ emulsion of Eudragit RS100 particles, prepared by using (a) ultra turrax (UT) and (b) ultrasound (US) in the secondary step.

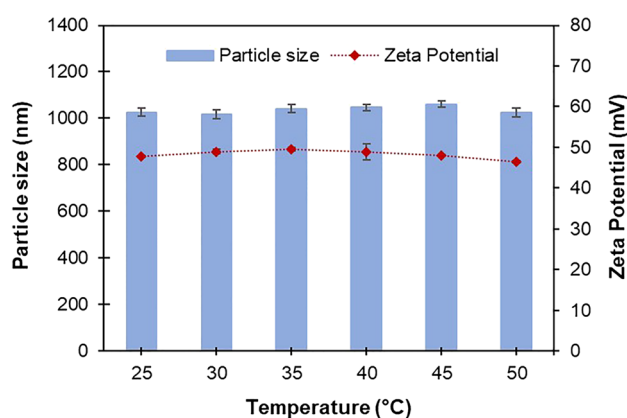


Figure 4. Average size and zeta potential of PNIPAM@RS100 measured at different temperatures.

a high-energy ultrasound (US). The results on the average size and size distribution are summarized in Fig. 3. The nanodroplets in the primary emulsion showed hydrodynamic diameters between 90 and 950 nm with a PDI value of 0.2, reflecting monodispersed emulsion. The high-energy sonication was employed to produce uniform and smaller droplets in the primary emulsion relative to the larger counterparts obtained in the double emulsion process. Nevertheless, the small droplet size does not affect the final particle size in the secondary emulsification^{21,39}. The energy required to form secondary emulsion was provided to the system by UT and US to avoid aggregation and enhance particle dispersion.

The utilization of UT produced microparticles with an average particle size of 1750 nm and a PDI value of 0.4 (Fig. 3a). In contrast, when US was applied in the secondary emulsion process, nanoparticles with an average size of 460 nm and narrow size distribution (PDI value of 0.2) were produced, as shown in Fig. 3b. Although both nano- and microparticles showed high colloidal stability at ambient temperature, the colloidal microparticles fabricated by UT precipitated after 7 days, likely due to the gravitational force, as shown in Supplementary Fig. S5. However, the microparticle sediment can be easily re-dispersed upon shaking or agitation. In contrast, the smaller nanoparticles are well-dispersed without sedimentation or aggregation^{21,40,41}.

The obtained emulsions are stable without any stabilizer, which was confirmed by a high zeta potential value of $> +40$ mV, because of the positively-charged nature of Eudragit RS100. The incorporation of PNIPAM didn't significantly affect the zeta potential value of the particles. The zeta potential values of neat Eudragit RS100 and PNIPMA nanogels were observed at +48 mV and -15 mV, respectively. The change in temperatures also did not affect the particle size and zeta potential of PNIPAM@RS100, as shown in Fig. 4. This is because the matrix domain of these particles is derived from porous Eudragit RS100, which is not sensitive to temperature changes. It is noted that the cationic macromolecule Eudragit RS100 could interact with anionic components (*N*-acetylneuraminic acid) of glycoprotein on the surface of cells. However, the materials are non-toxic to human cells. Lopodota et al. examined the *in vitro* cytotoxicity of Eudragit RS100 (zeta potential of +40.5 mV) with a concentration in the range of 0–500 $\mu\text{g/mL}$ on human epithelial cells (HaCaT) and murine monocyte-macrophage cells (RAW 264.7)⁴². The authors reported no detectable cytotoxicity after 48 and 72 h of incubation.

Sample	Particle size (nm)	PDI	Zeta potential (mV)	Conversion (%)
UT-APS	1679 ± 81	0.47	48.3 ± 0.4	66.7 ± 0.5
UT-APS/TEMED	1729 ± 88	0.65	48.8 ± 0.5	77.3 ± 1.9
US-APS	415 ± 3	0.22	47.7 ± 0.8	69.9 ± 1.9
US-APS/TEMED	430 ± 7	0.15	47.8 ± 0.2	84.0 ± 2.2

Table 1. Average particle size, polydispersity index (PDI), zeta potential, and the conversion percentage of NIPAM monomer during the preparation of PNIPAM@RS100 particles. Mean ± SD, n = 3, SD: standard deviation.

The polymerization of thermally-sensitive PNIPAM gatekeepers takes place during the PNIPAM@RS100 preparation step by a free radical polymerization. The effect of initiators on the degree of polymerization of NIPAM was investigated at 60 °C for a thermal initiator (APS) (referred to PNIPAM@RS100-APS), and at room temperature for redox initiators (referred to PNIPAM@RS100-APS/TEMED). The redox initiator system was used to initiate the polymerization below the decomposition temperature of APS⁴³. A small amount of TEMED catalyst was added into the inner aqueous phase (W_1). The catalyst can help enhance the polymerization rate by decreasing the activation energy (E_a) of the reaction at room temperature⁴⁴. The redox initiator system was employed to polymerize PNIPAM networks at room temperature. The APS/TEMED redox pair (ratio 1:1) generated the primary initiating radicals ($\text{HSO}_3\text{O}^\bullet$ and $(\text{CH}_3)_2\text{NCH}_2\text{CH}_2\text{N}^\bullet(\text{CH}_3)_2$), and hydroxyl free radicals (OH^\bullet) via a charge transfer complex and cyclic transition state in water medium^{44,45}. These reactive species initiated the NIPAM monomers and MBA crosslinker. A chain propagation of NIPAM then creates chain entanglements and covalent crosslinking of the PNIPAM structures (Supplemental Fig. S6). With the addition of TEMED, the percent conversions of NIPAM monomer to polymer were enhanced, while the particle diameter, polydispersity index, and zeta potential of both emulsions are in the same range, as summarized in Table 1.

The materials are designed to contain 20% w/w of PNIPAM in the Eudragit RS100 matrix. The feed concentration of NIPAM monomer in water was fixed at 1 wt/v% for all samples⁴⁶. Under the redox system, high concentrations of PNIPAM were incorporated in the pores of Eudragit RS100 (15.5 and 16.8%), while 13.3 and 14.0% were obtained for the thermal system counterpart, using UT and US methods, respectively. The resulting PNIPAM contents may be correlated with the porous particle formation and hence their thermo-responsive properties. To confirm this hypothesis, the morphology of the porous particles and thermoresponsive particles prepared by thermal and redox initiators are compared in Fig. 5. Spherical particles with large cavities and smooth surfaces were obtained in the UT system. After the polymerization, some cavities were closed or covered with a rough surface, likely derived from crosslinked PNIPAM domains. In contrast, PNIPAM@RS100-APS showed growing polymer chains enveloping the particles, as PNIPAM was polymerized after the particle formation. This is because the hydrophilic chains tend to move out to the aqueous medium, as they are allowed extensive time for polymerization. In the redox initiating system (PNIPAM@RS100-APS/TEMED), however, the PNIPAM nanogels were polymerized during the W/O formation in the first stage. The proposed formation mechanism of PNIPAM gatekeepers is shown in Fig. 6. In the US process, the high vibrational energy induced cavitation in the double emulsion process. TEM images show that neat Eudragit particles have a smooth surface and a large cavity inside the particles. The functionalized PNIPAM particles, however, exhibited rough surfaces, as the PNIPAM chains were present both inside and at the surface of the nanoparticles.

The coexistence of Eudragit RS100 and PNIPAM gates is confirmed by ATR-FTIR spectroscopy, as shown in Fig. 7. The spectrum of neat porous particles shows the characteristic band at 1725 cm^{-1} , corresponding to the stretching mode of C=O of Eudragit RS100⁴⁷. PNIPAM nanogels show bands at 1640 and 1537 cm^{-1} , corresponding to the amide I (C=O stretching) and amide II (N–H bending) modes, respectively⁴⁸. The corresponding spectra of thermoresponsive particles PNIPAM@RS100 were almost identical to that of neat Eudragit RS100 particles. The appearance of the amide I and II bands confirms the formation of PNIPAM gatekeepers on the porous particles from the conversion of the NIPAM monomer.

Encapsulation and in vitro release of Nile Blue A (NB). To investigate the encapsulation efficiency and release behavior of PNIPAM@RS100-APS/TEMED, a fluorescent dye NB is chosen as a model compound. The dye also serves as a pH-sensitive probe, whose colorimetric reversibly changes from blue to pink, depending on acidic or basic ($\text{pH} > 7.6$) environments by the protonation/deprotonation of its amino groups and the rearrangements of its conjugate system⁴⁹. The cationic charge transfer structures of NB are demonstrated in Fig. 8.

The encapsulation of the NB model in PNIPAM@RS100 particles was conducted by direct encapsulation during the particle's formation step. NB was uniformly distributed and covered with crosslinked PNIPAM gatekeepers. The encapsulation efficiency (%EE) and loading capacity (%LC) of NB were calculated according to Eqs. (4) and (5), as summarized in Fig. 9. The encapsulation efficiency is dependent on the presence of the PNIPAM gating systems, especially those prepared by US. Given the same NB feed content of 0.2 mg for all samples, the nanoparticles prepared by US showed 92%EE and 36%LC for US-APS/TEMED, 66%EE and 27%LC for US-APS, and 32%EE and 13%LC for neat porous particles. In contrast, the microparticles prepared by UT showed 89%EE and 36%LC for UT-APS/TEMED, 88%EE and 35%LC for UT-APS, and 78%EE and 32%LC for neat porous particles. This implies that the presence of PNIPAM gatekeepers is essential to effectively entrap NB inside PNIPAM@RS100. In the microparticle system, high encapsulation efficiency was observed due to the large pore volume that could encapsulate a high amount of NB in their porous structure. In addition, the type of

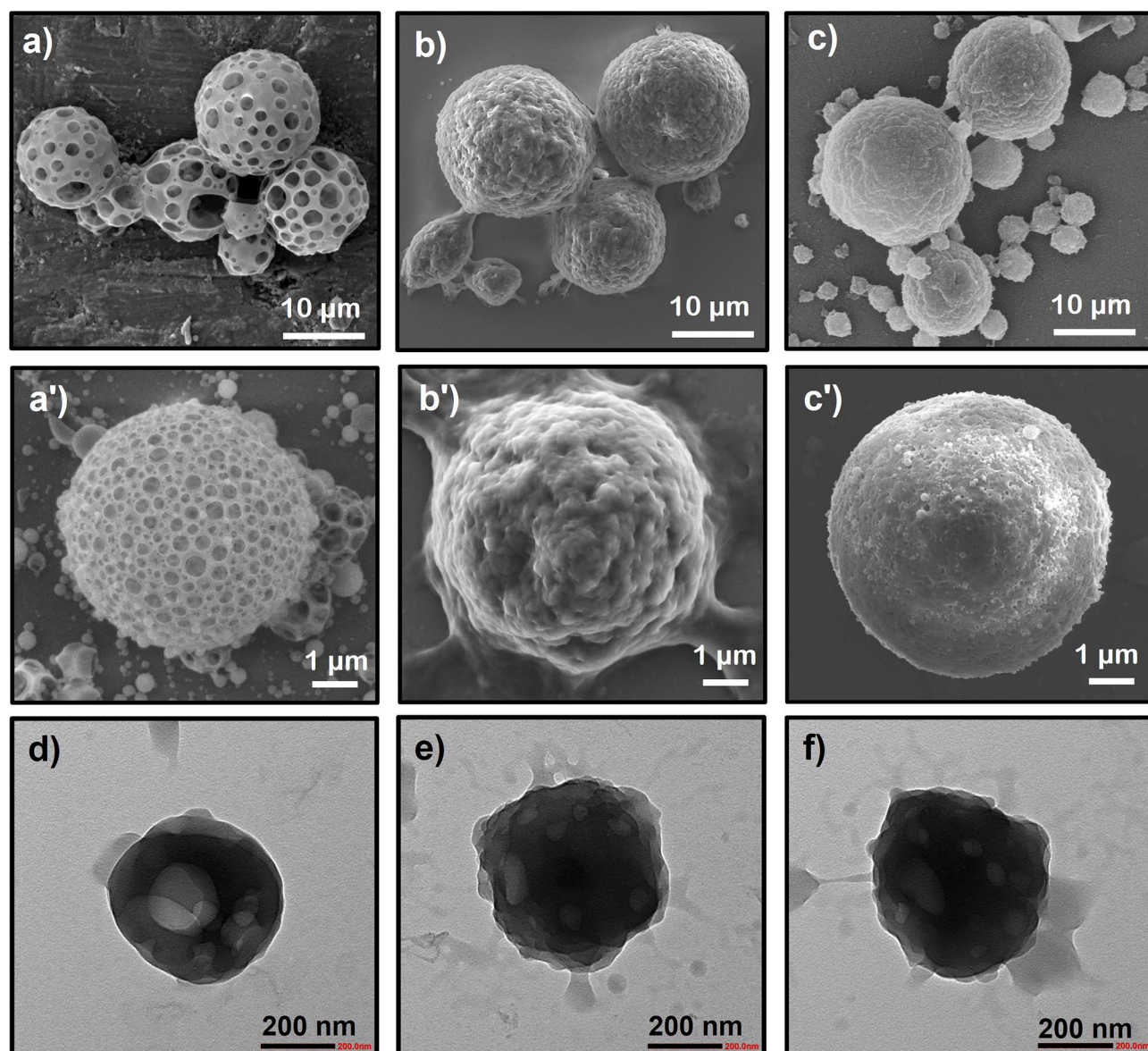


Figure 5. SEM images of Eudragit RS100 porous particles and PNIPAM@RS100 prepared by ultra turrax; (a,a') UT-RS100, (b,b') UT-APS, (c,c') UT-APS/TEMED, and TEM images of nanoparticles prepared by ultrasonication; (d) US-RS100, (e) US-APS, (f) US-APS/TEMED. The images were taken at 5kX (a–c), 10kX (a'–c') and 25kX (d–f) magnifications.

initiators used in the PNIPAM polymerization plays a key role in the encapsulation efficiency. The results from the redox-initiated system of PNIPAM gatekeeper's formation strongly support an assumption that the addition of TEMED helps to improve the polymerization rate of the crosslinked PNIPAM, resulting in the highest effective gatekeepers in the entrapment of NB.

The temperature-sensitive gating behavior of the biodegradable porous particles was studied by monitoring the release of the NB model. In the thermal-initiating system, NB encapsulated in PNIPAM@RS100-APS emulsion is blue due to the acidic environment (pH of 3.4). In contrast, a pink emulsion was observed in the redox-initiating counterpart (PNIPAM@RS100-APS/TEMED) because of the contact between NB and basic TEMED (pH of 8.9). From visual inspection, the NB-loaded colloidal particles changed from pink to blue when the temperature was increased above T_{VPT} , as the entrapped NB (pink form) was released to a neutral medium (blue form). To evaluate the performance of the crosslinked PNIPAM gatekeepers, the NB release profiles from PNIPAM@RS100 carriers were examined at room temperature (25 °C, below T_{VPT}) and the human body temperature (37 °C, above T_{VPT}). A spectrometer was employed to monitor the kinetic release of NB as a function of time. The cumulative release of NB from thermoresponsive particles measured at 25 and 37 °C is summarized in Fig. 10. The results indicate an initial burst release in the early state (5 min), followed by a diffusive release. The zero-order kinetic release indicated a drug diffusion-controlled mechanism through PNIPAM gatekeepers and the particle cavities. The released NB at room temperature was around 50%. By increasing the temperature

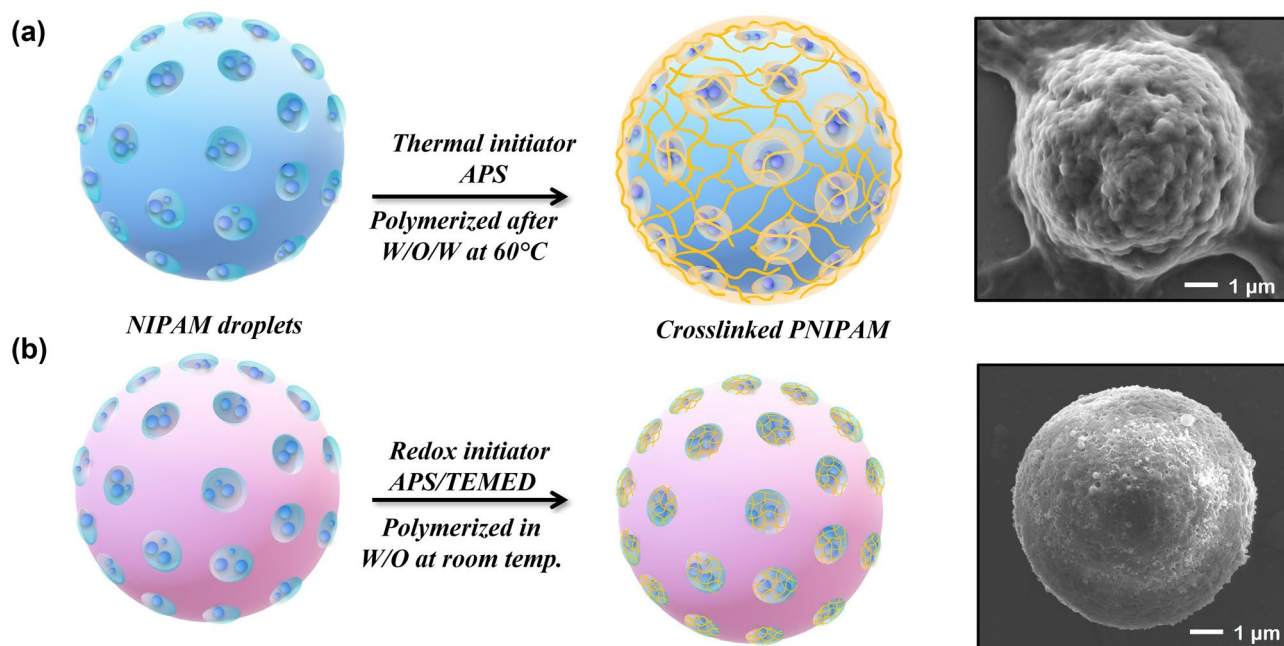


Figure 6. Schematic of the formation mechanisms of PNIPAM gatekeepers on porous Eudragit particles by using different initiators; (a) thermal and (b) redox initiators.

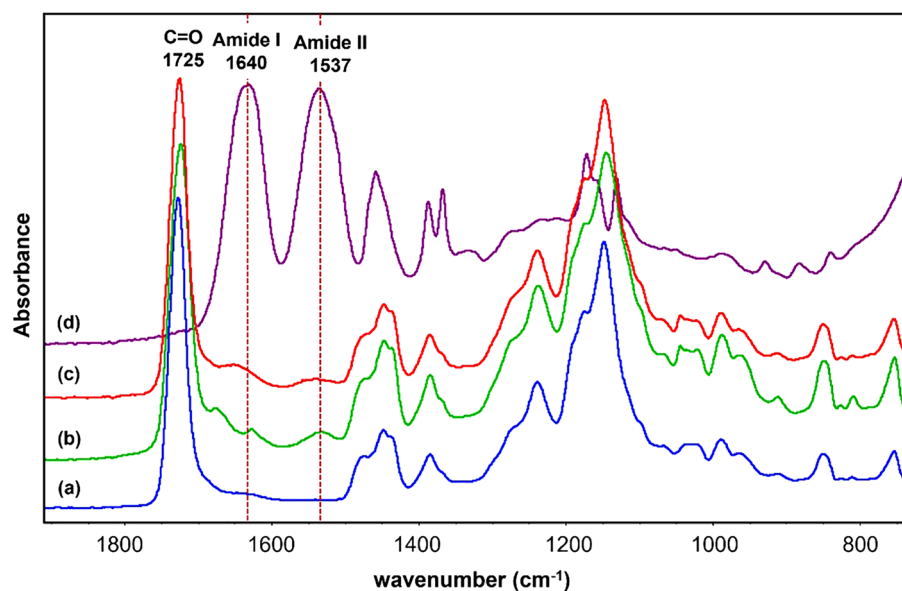


Figure 7. ATR-FTIR spectra of (a) neat Eudragit RS100 porous particles, (b) PNIPAM@RS100-APS, (c) PNIPAM@RS100-APS/TEMED, and (d) PNIPAM nanogels.

above T_{VPT} , the cumulative release rate increased as the crosslinked PNIPAM collapsed, causing the opening of gatekeepers. The loaded NB in US-PNIPAM@RS100 was released at a higher rate and reached 100% within one h. For microparticles with larger pore sizes, UT-PNIPAM@RS100 showed a prolonged release mechanism. The results agree with Chen et al. on the effect of particle size on the in vitro release of PLGA particles¹¹. The size-fractionated particles showed different drug release rates, i.e., small size particles exhibited a rapid diffusion and a complete release within one week, while larger microspheres showed slower release for more than three months. This suggested that the diffusion rate of the entrapped drug trapped inside the cavity is correlated with the diffusion path lengths between the interior cavity and the wall-cavity interface.

After the complete release experiments at 25 and 37 °C, the morphology of all NB-encapsulated particles remained unchanged, as evidenced in Supplementary Fig. S7. This is due to the high thermal stability of their Eudragit RS100 matrix. Given that Eudragit RS100 has a glass transition temperature (T_g) at 57 °C, the material

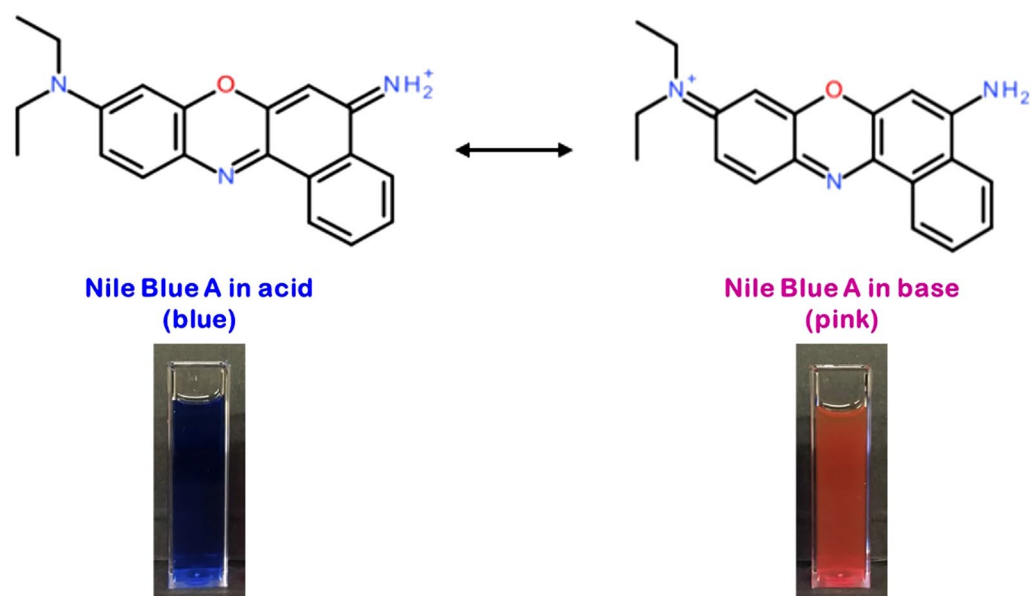


Figure 8. Reversible protonation and deprotonation states of Nile Blue A.

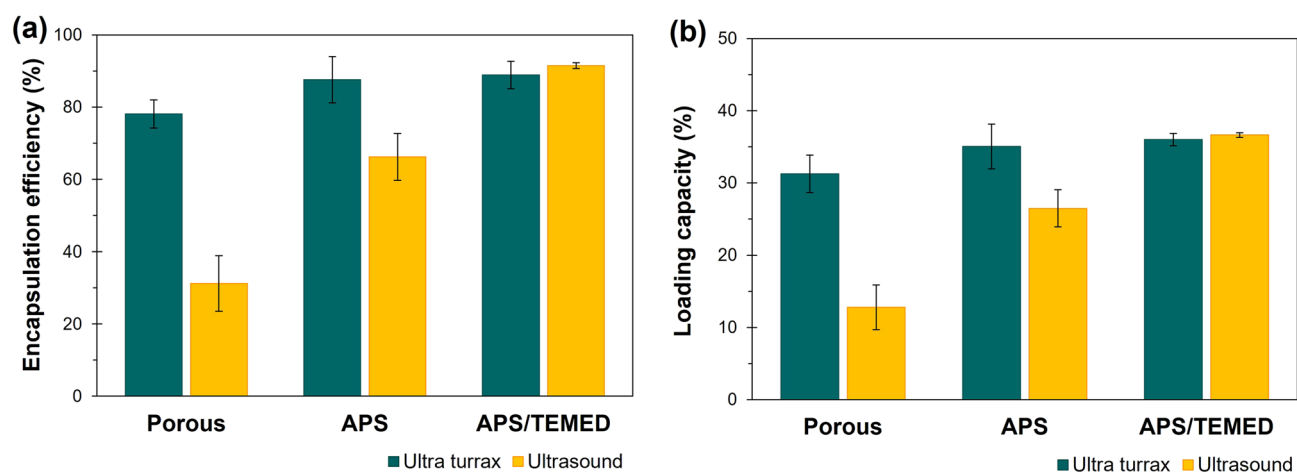
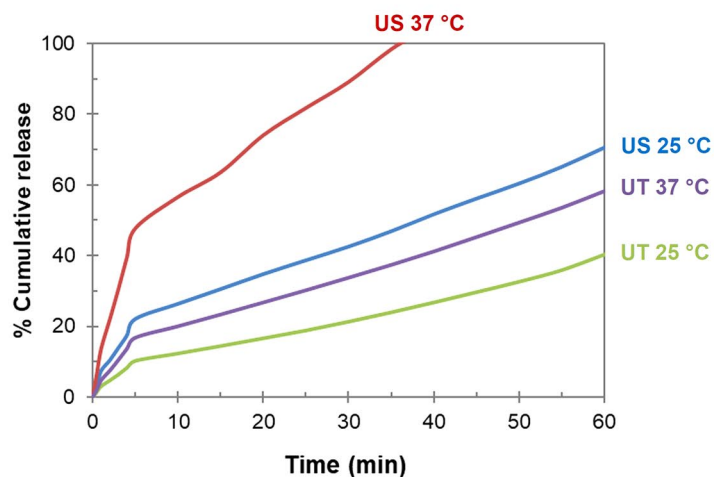
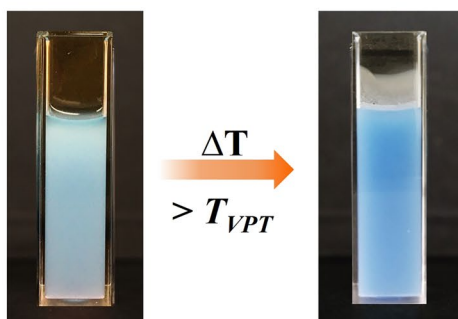


Figure 9. Comparative study of (a) encapsulation efficiency and (b) loading capacity of Nile blue A-loaded particles prepared by ultra turrax (UT) and ultrasound (US) in the second step.

remains in a glassy state throughout the temperature range. This confirms that the crosslinked PNIPAM gatekeepers play a key role in controlling the release of the model compound when triggered by temperature changes.

In medical applications, especially hyperthermia cancer treatments, a precise and rapid drug release is essential when the materials are triggered, rather than a steady release, because a high dose is required to kill the tumor cells⁵⁰. As PNIPAM has T_{VPT} at 32.8 °C, the temperatures in the ranges enveloped at this point can be used to stimulate its gating behavior. To demonstrate a precise control of the gatekeeping mechanism, a temperature pair with a sufficiently large difference within the normal body temperature range is chosen at 4 and 40 °C. The nanoparticles prepared by the US method were examined, as shown in Fig. 11. The release behavior is also demonstrated as video supplemental data. These phenomena are related to the pore structure of the particles and the responsive behavior of the polymeric gatekeepers. When the temperature was increased above T_{VPT} (40 °C), as “turn on”, the collapsed PNIPAM network allowed NB to diffuse out (ca. 25% during a period of 5 min). The gatekeeper was then “closed” by cooling down to 4 °C. A similar amount of NB was further released when the materials were reheated to 40 °C in the following cycles. Although a trace amount of NB was released due to delayed movements of the closing gates, the constant release rate reflects a well-defined release mechanism. Almost all NB was released after four cycles of experiments, indicating complete removal of the encapsulated compound.

(a) Thermal initiating system



(b) Redox initiating system

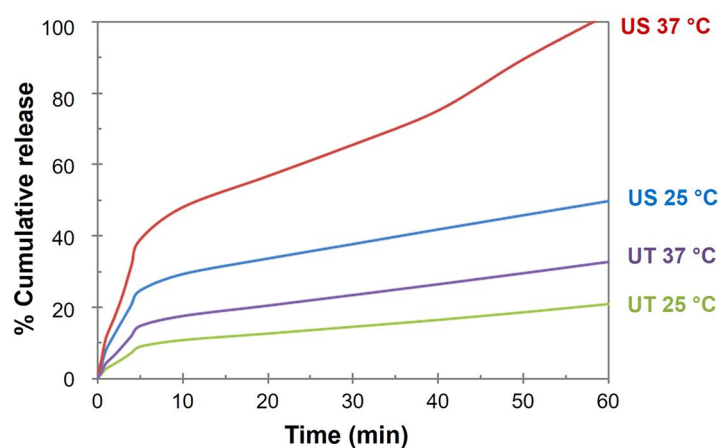
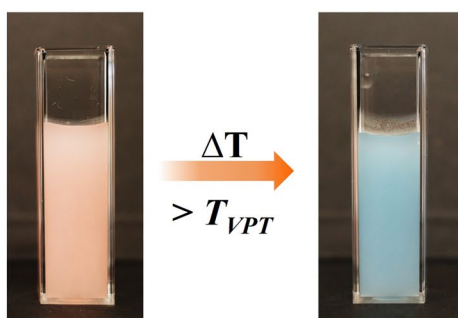


Figure 10. Thermoresponsive behavior of PNIPAM@RS100; visual observation of color change of emulsions and cumulative release of Nile Blue A at room temperature (25 °C) and the body temperature (37 °C) in DI water. The PNIPAM gating particles were prepared by (a) thermal and (b) redox initiating systems.

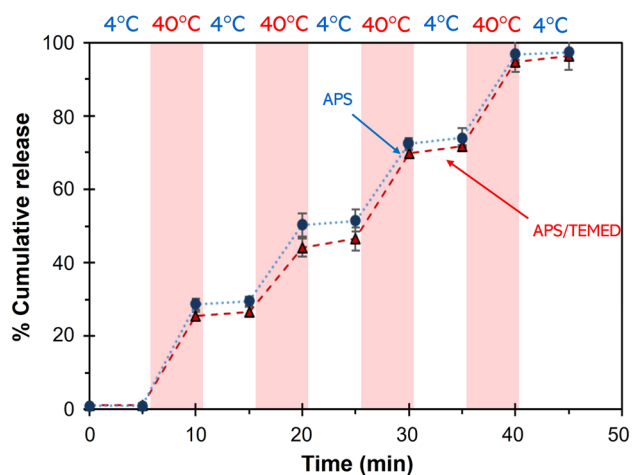


Figure 11. Switchable release profiles of US-PNIPAM@RS100.

Conclusions

Thermoresponsive PNIPAM network has been demonstrated as an effective gatekeeper for biodegradable porous particles of Eudragit RS100 to entrap and release a model compound (NB). The porous particles functionalized with PNIPAM gatekeepers were synthesized by a facile in situ formation *via* a double emulsion solvent evaporation. The reaction time is much shorter than other reported multi-step processes, consisting of several particle formation steps and functionalization with stimuli-responsive agents. The employment of a redox-initiated system (APS/TEMED) in the fabrication of the nanoparticles improved the gatekeeper formation and encapsulation efficiency (92%). The NB-loaded PNIPAM@RS100-APS/TEMED particles were selected to demonstrate a switchable “close-open” response mechanism of the temperature-sensitive gates. Colorimetric change (pink to blue) of the emulsion of NB-loaded particles reflected the collapsed gates and drug diffusion. The gatekeeper’s switchable open/close mechanisms can be accurately controlled to release the loaded compound at a constant rate until completion. The results indicate that the PNIPAM@RS100 thermoresponsive system is a promising candidate for controlled drug delivery materials at the human body temperature, with a precise and easy triggering mechanism.

Received: 5 April 2022; Accepted: 17 June 2022

Published online: 28 June 2022

References

- Jiao, J. *et al.* Redox and pH dual-responsive PEG and chitosan-conjugated hollow mesoporous silica for controlled drug release. *Mater. Sci. Eng. C* **67**, 26–33. <https://doi.org/10.1016/j.msec.2016.04.091> (2016).
- Gao, W., Chan, J. M. & Farokhzad, O. C. pH-responsive nanoparticles for drug delivery. *Mol. Pharm.* **7**, 1913–1920. <https://doi.org/10.1021/mp100253e> (2010).
- Qiao, S. & Wang, H. Temperature-responsive polymers: Synthesis, properties, and biomedical applications. *Nano Res.* **11**, 5400–5423. <https://doi.org/10.1007/s12274-018-2121-x> (2018).
- Medeiros, S. F., Santos, A. M., Fessi, H. & Elaissari, A. Stimuli-responsive magnetic particles for biomedical applications. *Int. J. Pharm.* **403**, 139–161. <https://doi.org/10.1016/j.ijpharm.2010.10.011> (2011).
- Hao, Y., Meng, J. & Wang, S. Photo-responsive polymer materials for biological applications. *Chin. Chem. Lett.* **28**, 2085–2091. <https://doi.org/10.1016/j.ccl.2017.10.019> (2017).
- Cai, D. *et al.* Chitosan-capped enzyme-responsive hollow mesoporous silica nanoplateforms for colon-specific drug delivery. *Nanoscale Res. Lett.* **15**, 123. <https://doi.org/10.1186/s11671-020-03351-8> (2020).
- Colson, Y. L. & Grinstaff, M. W. Biologically responsive polymeric nanoparticles for drug delivery. *Adv. Mater.* **24**, 3878–3886. <https://doi.org/10.1002/adma.201200420> (2012).
- Moore, T. L. *et al.* Shape-specific microfabricated particles for biomedical applications: A review. *Drug Deliv. Transl. Res.* <https://doi.org/10.1007/s13346-022-01143-4> (2022).
- Islam, M. A., Barua, S. & Barua, D. A multiscale modeling study of particle size effects on the tissue penetration efficacy of drug-delivery nanoparticles. *BMC Syst. Biol.* **11**, 113–113. <https://doi.org/10.1186/s12918-017-0491-4> (2017).
- Mandrachia, D. & Tripodo, G. *Silk-based Drug Delivery Systems* 1–24 (The Royal Society of Chemistry, 2021).
- Chen, W., Palazzo, A., Hennink, W. E. & Kok, R. J. Effect of particle size on drug loading and release kinetics of gefitinib-loaded PLGA microspheres. *Mol. Pharm.* **14**, 459–467. <https://doi.org/10.1021/acs.molpharmaceut.6b00896> (2017).
- Kim, I. *et al.* Doxorubicin-loaded porous PLGA microparticles with surface attached TRAIL for the inhalation treatment of metastatic lung cancer. *Biomaterials* **34**, 6444–6453. <https://doi.org/10.1016/j.biomaterials.2013.05.018> (2013).
- Reczynska, K. *et al.* Stimuli-sensitive fatty acid-based microparticles for the treatment of lung cancer. *Mater. Sci. Eng. C* **111**, 110801. <https://doi.org/10.1016/j.msec.2020.110801> (2020).
- Tian, Z. *et al.* Magnetic mesoporous silica nanoparticles coated with thermo-responsive copolymer for potential chemo- and magnetic hyperthermia therapy. *Microporous Mesoporous Mater.* **256**, 1–9. <https://doi.org/10.1016/j.micromeso.2017.07.053> (2018).
- Cho, I.-H. *et al.* Heat shock responsive drug delivery system based on mesoporous silica nanoparticles coated with temperature sensitive gatekeeper. *Microporous Mesoporous Mater.* **253**, 96–101. <https://doi.org/10.1016/j.micromeso.2017.06.042> (2017).
- Martins, I. M., Barreiro, M. F., Coelho, M. & Rodrigues, A. E. Microencapsulation of essential oils with biodegradable polymeric carriers for cosmetic applications. *Chem. Eng. J.* **245**, 191–200. <https://doi.org/10.1016/j.cej.2014.02.024> (2014).
- Zhou, M., Shen, L., Lin, X., Hong, Y. & Feng, Y. Design and pharmaceutical applications of porous particles. *RSC Adv.* **7**, 39490–39501. <https://doi.org/10.1039/C7RA06829H> (2017).
- Yang, P., Gai, S. & Lin, J. Functionalized mesoporous silica materials for controlled drug delivery. *Chem. Soc. Rev.* **41**, 3679–3698. <https://doi.org/10.1039/C2CS15308D> (2012).
- Son, H. Y. *et al.* In situ functionalization of highly porous polymer microspheres with silver nanoparticles via bio-inspired chemistry. *RSC Adv.* **4**, 55604–55609. <https://doi.org/10.1039/C4RA08685F> (2014).
- Amoyav, B. & Benny, O. Microfluidic based fabrication and characterization of highly porous polymeric microspheres. *Polymers* **11**, 419. <https://doi.org/10.3390/polym11030419> (2019).
- Zafar, N., Bitar, A., Valour, J. P., Fessi, H. & Elaissari, A. Elaboration of ammonio methacrylate copolymer based spongy cationic particles via double emulsion solvent evaporation process. *Mater. Sci. Eng. C* **61**, 85–96. <https://doi.org/10.1016/j.msec.2015.12.017> (2016).
- Constantin, M., Cristea, M., Ascenzi, P. & Fundueanu, G. Lower critical solution temperature versus volume phase transition temperature in thermoresponsive drug delivery systems. *EXPRESS Polym. Lett.* **5**, 839–848. <https://doi.org/10.3144/expresspolymlett.2011.83> (2011).
- Wu, T.-Y., Zrimsek, A. B., Bykov, S. V., Jakubek, R. S. & Asher, S. A. Hydrophobic collapse initiates the poly(N-isopropylacrylamide) volume phase transition reaction coordinate. *J. Phys. Chem. B* **122**, 3008–3014. <https://doi.org/10.1021/acs.jpcc.8b00740> (2018).
- Su, Y. *et al.* Thermoresponsive coatings on hollow particles with mesoporous shells serve as stimuli-responsive gates to species encapsulation and release. *Langmuir* **34**, 14608–14616. <https://doi.org/10.1021/acs.langmuir.8b02714> (2018).
- Galperin, A., Long, T. J., Garty, S. & Ratner, B. D. Synthesis and fabrication of a degradable poly(N-isopropyl acrylamide) scaffold for tissue engineering applications. *J. Biomed. Mater. Res.* **101A**, 775–786. <https://doi.org/10.1002/jbm.a.34380> (2013).
- Capella, V. *et al.* Cytotoxicity and bioadhesive properties of poly-N-isopropylacrylamide hydrogel. *Heliyon* **5**, e01474. <https://doi.org/10.1016/j.heliyon.2019.e01474> (2019).
- Naha, P. C. *et al.* Intracellular localisation, geno- and cytotoxic response of polyN-isopropylacrylamide (PNIPAM) nanoparticles to human keratinocyte (HaCaT) and colon cells (SW 480). *Toxicol. Lett.* **198**, 134–143. <https://doi.org/10.1016/j.toxlet.2010.06.011> (2010).

28. Khorasani, R. & Pourmahdian, S. Synthesis and characterization of hydrogel nanoparticles through inverse microemulsion polymerization of 2-acrylamido-2-methyl-1-propanesulfonic acid. *J. Macromol. Sci. Part A* **51**, 240–248. <https://doi.org/10.1080/10601325.2014.871955> (2014).
29. Kim, Y. K. *et al.* Dual stimuli-triggered nanogels in response to temperature and pH changes for controlled drug release. *Nanoscale Res. Lett.* **14**, 77. <https://doi.org/10.1186/s11671-019-2909-y> (2019).
30. López-León, T., Ortega-Vinuesa, J. L., Bastos-González, D. & Elaissari, A. Cationic and anionic poly(N-isopropylacrylamide) based submicron gel particles: Electrokinetic properties and colloidal stability. *J. Phys. Chem. B* **110**, 4629–4636. <https://doi.org/10.1021/jp0540508> (2006).
31. Tavagnacco, L., Zaccarelli, E. & Chiessi, E. On the molecular origin of the cooperative coil-to-globule transition of poly(N-isopropylacrylamide) in water. *Phys. Chem. Chem. Phys.* **20**, 9997–10010. <https://doi.org/10.1039/C8CP00537K> (2018).
32. Burmistrova, A., Richter, M., Uzum, C. & Klitzing, R. V. Effect of cross-linker density of P(NIPAM-co-AAc) microgels at solid surfaces on the swelling/shrinking behaviour and the Young's modulus. *Colloid Polym. Sci.* **289**, 613–624. <https://doi.org/10.1007/s00396-011-2383-2> (2011).
33. Varga, I., Gilányi, T., Mészáros, R., Filipcsei, G. & Zrínyi, M. Effect of cross-link density on the internal structure of poly(N-isopropylacrylamide) microgels. *J. Phys. Chem. B* **105**, 9071–9076. <https://doi.org/10.1021/jp004600w> (2001).
34. Khan, A. *et al.* Semibath polymerization approach for one-pot synthesis of temperature- and glucose-responsive core-shell nanogel particles. *J. Nanomater.* **2018**, 2180518. <https://doi.org/10.1155/2018/2180518> (2018).
35. Fernández-Nieves, A., Fernández-Barbero, A., De las Nieves, F. J. & Vincent, B. Motion of microgel particles under an external electric field. *J. Phys. Condens. Matter* **12**, 3605–3614. <https://doi.org/10.1088/0953-8984/12/15/309> (2000).
36. Maki, Y., Sugawara, K. & Nagai, D. Temperature dependence of electrophoretic mobility and hydrodynamic radius of microgels of poly(N-isopropylacrylamide). *Gels* **4**, 37 <https://doi.org/10.3390/gels4020037> (2018).
37. Pelton, R. H., Pelton, H. M., Morphesis, A. & Rowell, R. L. Particle sizes and electrophoretic mobilities of poly(N-isopropylacrylamide) latex. *Langmuir* **5**, 816–818. <https://doi.org/10.1021/la00087a040> (1989).
38. Nabzar, L., Duracher, D., Elaissari, A., Chauveteau, G. & Pichot, C. Electrokinetic properties and colloidal stability of cationic amino-containing N-isopropylacrylamide–styrene copolymer particles bearing different shell structures. *Langmuir* **14**, 5062–5069. <https://doi.org/10.1021/la980244l> (1998).
39. Zafar, N., Agusti, G., Fessi, H. & Elaissari, A. Elaboration of sponge-like biodegradable cationic particles via double-emulsion solvent evaporation. *J. Dispers. Sci. Technol.* **38**, 577–583. <https://doi.org/10.1080/01932691.2016.1182923> (2017).
40. Wu, L., Zhang, J. & Watanabe, W. Physical and chemical stability of drug nanoparticles. *Adv. Drug Deliv. Rev.* **63**, 456–469. <https://doi.org/10.1016/j.addr.2011.02.001> (2011).
41. Iqbal, M., Valour, J.-P., Fessi, H. & Elaissari, A. Preparation of biodegradable PCL particles via double emulsion evaporation method using ultrasound technique. *Colloid Polym. Sci.* **293**, 861–873. <https://doi.org/10.1007/s00396-014-3464-9> (2015).
42. Lopedota, A. *et al.* The use of Eudragit® RS 100/cyclodextrin nanoparticles for the transmucosal administration of glutathione. *Eur. J. Pharm. Biopharm.* **72**, 509–520. <https://doi.org/10.1016/j.ejpb.2009.02.013> (2009).
43. Hu, X., Tong, Z. & Lyon, L. A. Control of poly(N-isopropylacrylamide) microgel network structure by precipitation polymerization near the lower critical solution temperature. *Langmuir* **27**, 4142–4148. <https://doi.org/10.1021/la200114s> (2011).
44. Strachota, B. *et al.* Poly(N-isopropylacrylamide)–clay based hydrogels controlled by the initiating conditions: Evolution of structure and gel formation. *Soft Matter* **11**, 9291–9306. <https://doi.org/10.1039/C5SM01996F> (2015).
45. Tsanaktisidou, E., Kammona, O. & Kiparissides, C. On the synthesis and characterization of biofunctional hyaluronic acid based injectable hydrogels for the repair of cartilage lesions. *Eur. Polym. J.* **114**, 47–56. <https://doi.org/10.1016/j.eurpolymj.2019.02.024> (2019).
46. Kakar, M. U. *et al.* Synthesis of bimetallic nanoparticles loaded on to PNIPAM hybrid microgel and their catalytic activity. *Sci. Rep.* **11**, 14759. <https://doi.org/10.1038/s41598-021-94177-6> (2021).
47. Barzegar-Jalali, M. *et al.* Comparison of physicochemical characteristics and drug release of diclofenac sodium–eudragit® RS100 nanoparticles and solid dispersions. *Powder Technol.* **219**, 211–216. <https://doi.org/10.1016/j.powtec.2011.12.046> (2012).
48. Pruettiphap, M., Rempel, G. L., Pan, Q. & Kiatkamjornwong, S. Morphology and drug release behavior of N-isopropylacrylamide/acrylic acid copolymer as stimuli-responsive nanogels. *Iran. Polym. J.* **26**, 957–969. <https://doi.org/10.1007/s13726-017-0571-8> (2017).
49. Wang, X.-L., Sun, R., Zhu, W.-J., Sha, X.-L. & Ge, J.-F. Reversible absorption and emission responses of Nile blue and Azure derivatives in extreme acidic and basic conditions. *J. Fluoresc.* **27**, 819–827. <https://doi.org/10.1007/s10895-016-2017-7> (2017).
50. Seynhaeve, A. L. B., Amin, M., Haemmerich, D., van Rhooon, G. C. & ten Hagen, T. L. M. Hyperthermia and smart drug delivery systems for solid tumor therapy. *Adv. Drug Deliv. Rev.* **163–164**, 125–144. <https://doi.org/10.1016/j.addr.2020.02.004> (2020).

Acknowledgements

The authors gratefully acknowledge the financial support from the National Research Council of Thailand (NRCT), the NSRF *via* the Program Management Unit for Human Resources & Institutional Development, Research and Innovation (grant number B16F640084), and the Center of Excellence in Materials and Plasma Technology (CoE M@P Tech), Thammasat University. K. Thananukul gratefully acknowledges the scholarship support from the Royal Golden Jubilee (RGJ) Ph.D. program of the National Research Council of Thailand (PHD/0108/2560) and additional grants from the French Embassy in Thailand.

Author contributions

K.T. carried out all the experiments, analyzed all data, writing original draft preparation. A.E. and P.O. Corresponding authors, designed the experiment and got the funding, supervised the whole experiment process, reviewed and editing. C.K. and N.Z. guided the implementation of the experiment, review, and editing. All authors have read and agreed to the published version of the manuscript.

Competing interests

The authors declare no competing interests.

Additional information

Supplementary Information The online version contains supplementary material available at <https://doi.org/10.1038/s41598-022-15069-x>.

Correspondence and requests for materials should be addressed to P.O. or A.E.

Reprints and permissions information is available at www.nature.com/reprints.

Publisher's note Springer Nature remains neutral with regard to jurisdictional claims in published maps and institutional affiliations.



Open Access This article is licensed under a Creative Commons Attribution 4.0 International License, which permits use, sharing, adaptation, distribution and reproduction in any medium or format, as long as you give appropriate credit to the original author(s) and the source, provide a link to the Creative Commons licence, and indicate if changes were made. The images or other third party material in this article are included in the article's Creative Commons licence, unless indicated otherwise in a credit line to the material. If material is not included in the article's Creative Commons licence and your intended use is not permitted by statutory regulation or exceeds the permitted use, you will need to obtain permission directly from the copyright holder. To view a copy of this licence, visit <http://creativecommons.org/licenses/by/4.0/>.

© The Author(s) 2022